Applied Catalysis B: Environmental 129 (2013) 606–613

Contents lists available at SciVerse ScienceDirect

Applied Catalysis B: Environmental

journal homepage: www.elsevier.com/locate/apcatb

Fabrication of CNTs and GP/AuGP modified TiO_2 photocatalyst with two-channel electron conduction path for significantly enhanced photocatalytic activity

Wei Wang, Chunhua Lu*, Yaru Ni, Zhongzi Xu

State Key Laboratory of Materials-Orient Chemical Engineering, College of Materials Science and Engineering, Nanjing University of Technology, Nanjing 210009, PR China

ARTICLE INFO

Article history:
Received 17 July 2012
Received in revised form 9 October 2012
Accepted 14 October 2012
Available online 23 October 2012

Keywords:
Graphene
Carbon nanotube
TiO_2
Au deposition
Photoactivity

ABSTRACT

A systematic study has been devoted to fabricate carbon nanotubes (CNTs), graphene (GP), and Au deposited graphene (AuGP) modified semiconductor photocatalysts with specific structures. We show a systematic investigation on improving the photocatalytic activity of TiO_2 via a strategy of locating CNTs inside and GP/AuGP outside TiO_2 nanoparticles, respectively. To enhance the interaction between TiO_2 and CNTs/GP/AuGP, TiO_2 was directly grown on the surface of CNTs and GP/AuGP was covered on the entire surface of CNTs modified TiO_2 by the hydrothermal method. Au was used to fabricate a Schottky barrier on the TiO_2 and Au interface, resulting more efficient electron transfer by the Au particles and GP. The CNTs@TiO_2@GP and CNTs@TiO_2@AuGP nanocomposites which show higher photoactivity than P25 prepared by this method is able to make efficient use of the electron conductivity of Au, GP, and CNTs, resulting in more efficient transfer of the photogenerated electrons and, hence, inhibit the photogenerated electron–hole pair recombination, thus the solar energy was more efficiently used to decompose the pollutants. This simple method is of great significance for the design and preparation of high active photocatalysts with specific structures for pollutant decomposition.

1. Introduction

Titanium dioxide (TiO_2) is one of the most widely investigated semiconductor photocatalysts that performs photocatalytic activity and is used in a wide range of fields [1–3]. When TiO_2 is irradiated by the light with energy higher than its band gap, the electrons will get excited from the valence band (VB) to the conduction band (CB), both the produced electrons and holes will serve to the photocatalytic reactions. However, there are two main drawbacks of TiO_2 for efficient photocatalytic acitivity: (a) the large band gap induces its inability to make use of the visible light which contains about 45% of the solar light. Only about 4% of the solar energy in the UV range can be used for the photocatalytic reactions. (b) The rapid recombination rate of the photogenerated electrons and holes before they migrate to the surface of the photocatalyst to decompose pollutants. Therefore, in order to enhance the photocatalytic activity of TiO_2, the main challenge is to enhance the light absorption, prevent the rapid photogenerated electron–hole pair recombination.

A series of studies have been reported to synthesize TiO_2 photocatalysts for the enhancement of light absorption and the inhibition of electron–hole recombination [4,5]. For example, doping with metals and nonmetals [6–9], combining with semiconductors [10], and sensitizing with dyes and metal particles [11,12]. It has been reported that the deposition of Au particles show enhanced photocatalytic activity because of enhanced light absorption and electron transfer from TiO_2 to Au particles [13]. The Schottky barrier formed at the Au/TiO_2 interface is the main drive force for the inhibition of the electron–hole recombination [14]. The amount of Au particles and their particle size are also the factors affecting the photocatalytic activity of the Au deposited TiO_2 based photocatalysts.

Recently, the combination of carbon based materials, such as carbon nanotubes (CNTs) and graphene (GP), with TiO_2 to enhance the photocatalytic activity has been drawing much attention [15–17]. The introduction of CNTs and GP not only enhance the light absorption but also significantly enhance the electron transfer. To data, a lot of strategies, such as direct mixing, microwave, calcination, hydrothermal methods have been applied to prepare CNTs combined TiO_2 photocatalysts [18–21]. Well crystallized and particle sized controlled TiO_2 can always be synthesized by the hydrothermal method. In particular, the TiO_2/CNTs photocatalysts prepared from the TiO_2 seeds on CNTs with the hydrothermal method can give a tight interaction between TiO_2 and CNTs. As a result, the entire surface of CNTs will be covered by TiO_2, resulting more efficiency in electron transformation. Because of the exceptional electrical mobility (250,000 $cm^2/(Vs)$) property, GP has been investigated widely in photocatalytic applications [22,23]. Well crystallized and particle sized controlled TiO_2 can always be

* Corresponding author. Tel.: +86 25 83587220; fax: +86 25 83587252.
E-mail address: lchnjut@163.com (C. Lu).

0926-3373/$ – see front matter © 2012 Elsevier B.V. All rights reserved.
http://dx.doi.org/10.1016/j.apcatb.2012.10.014

synthesized by the hydrothermal method. In particular, the TiO_2/CNTs photocatalysts prepared from the TiO_2 seeds on CNTs with the hydrothermal method can give a tight interaction between TiO_2 and CNTs. As a result, the entire surface of CNTs will be covered by TiO_2, resulting in more electron transformation efficiency. Because of the hydrophobic property of GP, its modification of TiO_2 often results from the reduction of graphene oxide (GO), which is prepared with a modified Hummers method [24,25]. During the reduction process, the oxygen functional groups can serve as bridges to interact with the TiO_2 surface, resulting in significant photocatalytic activity enhancement. On the other hand, Zhang et al. has also observed that the GP supported SnO_2 and TiO_2 exhibited ability for the degradation of organic dyes under visible light irradiation [17]. The combination of CNTs and GP to modify TiO_2 has also been proposed recently. Shen et al. successfully synthesized the three-dimensional TiO_2-GP-CNTs nanocomposites [26]. The CNTs and GP were all physically mixed with TiO_2, which did not show much difference compared to that of single CNTs or GP modification. However, this method provides a new sight in enhancing the photocatalytic activity of TiO_2 based photocatalyst.

These pioneering works promote us to envision that, if the CNTs, TiO_2, and GP composited photocatalysts is fabricated in a structure of CNTs@TiO_2@GP, a much more efficient photocatalyst with enhanced photoactivity can be obtained. On the other hand, the deposition of Au particles between the interface of TiO_2 and GP will further enhance the electron transfer from the TiO_2 to GP. To verify whether this idea is feasible or not, we made a systematic investigation on the CNTs, GP, and AuGP modified TiO_2 photocatalysts. By the TiO_2 nanocrystalline seeds plantation on the CNTs surface, the CNTs@TiO_2 was synthesized by the hydrothermal method. Au particles were deposited on the 2D GO sheets successfully to produce the AuGO. Then GP, and AuGP modified CNTs@TiO_2 were prepared by the hydrothermal method. Also, Au and AuGP modified CNTs@TiO_2 and pure TiO_2 were prepared as the reference photocatalysts. Photocatalytic activity testing on degradation of methylene blue (MB) under the UV and visible light irradiation, respectively, demonstrates that the as-prepared CNTs@TiO_2@GP and CNTs@TiO_2@AuGP have enhanced the photoactivity as compared to CNTs@TiO_2 and the reference photocatalysts (TiO_2@AuGP and CNTs@TiO_2@Au). In addition, the photoactivity of CNTs@TiO_2@AuGP is much higher than that of CNTs@TiO_2@GP. Our present work significantly highlights the importance of designing more efficient CNTs-semiconductor-GP photocatalysts with the two-channel (inside and outside) electron conduction path. Still, the incorporation of Au particles enables further improved photocatalytic performance both under UV and visible light irradiation. Therefore, the efficient use of solar light to decompose organic contaminants by the photocatalysts can be widely used in a lot of applications in the future.

2. Experimental

2.1. Preparation of TiO_2 seeded CNTs

During the experimental process, CNTs (1 g) was dispersed in concentrated nitric acid (100 ml) by sonication, and then the suspension was kept at 100 °C for 4 h with continuous stirring. The purified CNTs was washed with deionized water and separated by centrifugation. After dried at 80 °C for 12 h, 20 mg of the purified CNTs were well-dispersed in 100 ml ethanol. 0.01 ml $Ti(OC_4H_9)_4$ was added into the obtained suspension, and then the suspension was magnetic stirred at room temperature until the ethanol was evaporated completely. At last, the product was grinded and annealed at 400 °C in air for 2 h with a temperature ramp rate of 3 °C/min to obtain the TiO_2 seeded CNTs.

2.2. Preparation of pure and Au loaded graphene oxide

GO was synthesized by the modified Hummers' method as reported by Zhang et al. [27]. To load the Au particles on GO, 3 ml $HAuCl_4$ aqueous solution (0.25 mg/ml) was mixed with 15 ml aqueous GO suspension (0.5 mg/ml). The mixture was magnetic stirred for 30 min at 90 °C, during which time the Au particles were deposited on the GO sheets to form AuGO.

2.3. Synthesis of the photocatalysts

Hydrothermal method was conducted to introduce TiO_2 nanoparticles on the whole surface of CNTs. Typically, 0.15 g TiO_2 seeded CNTs was dispersed in an aqueous solution containing 25 ml H_2O and 25 ml HCl (38%). Then 1 ml $Ti(OC_4H_9)_4$ was added into the suspension and stirred for 20 min, after which the suspension was transferred to a Teflon-lined autoclave (60 ml) and kept at 150 °C for 4 h. The CNTs modified TiO_2 (CNTs@TiO_2) was washed with deionized water, centrifuged, and dried. To produce the GP and AuGP modified CNTs@TiO_2, 0.15 g CNTs@TiO_2 was added into an aqueous suspension containing 20 ml ethanol, 20 ml H_2O, and 3 mg GO or AuGO. The mixture was transferred to the Teflon-lined autoclave, stirred for 60 min, and kept at 150 °C for 12 h. GO and AuGO were reduced to GP and AuGP during the hydrothermal process, and the resulted products were labeled as CNTs@TiO_2@GP and CNTs@TiO_2@AuGP, respectively. TiO_2 particles were prepared with same process that used to synthesize CNTs@TiO_2 in the absence of TiO_2 seeded CNTs. The location of Au on CNTs@TiO_2 (CNTs@TiO_2@Au) is similar to that which is used to prepare CNTs@TiO_2@AuGP in the absence of GO.

2.4. Characterization

Powder X-ray diffraction (XRD) measurements of as-obtained samples were conducted on an ARL X'TRA X-ray diffractometer using Cu K_α radiation (λ = 0.15406 nm) at a scanning rate of 5°/min. Filed emission scanning electron microscopy (FESEM) was performed with a S-4800 scanning electron analyzer with an accelerating voltage of 15 kV. Ultraviolet–visible (UV–vis) diffuse reflectance spectrum was performed with a 3101 spectrophotometer with $BaSO_4$ as the reflectance sample in the wavelength ranged from 200 to 700 nm. Photoluminescence (PL) emission spectrum was recorded on a FL3-221 fluorescence spectrophotometer equipped with a 450 W xenon lamp as the excitation source at room temperature (excitation wavelength λ_{ex} = 300 nm). The surface chemical environments were analyzed by X-ray photoelectron spectra (XPS) on a PHI5000 VersaProbe system with monochromatic Al Kα X-rays. Raman spectra were measured with a Labram HR800 spectrometer with 514 nm laser as the excitation source under ambient conditions. The FTIR spectra were recorded on a Vector-22 FTIR spectrometer in the range of 4000–400 cm^{-1}. TEM and HRTEM analysis were conducted on a JEM-2010 electron microscope (JEOL, Japan) at an accelerating voltage of 200 kV.

2.5. Photoactivity and •OH generation analysis

Photocatalytic activity measurements of the prepared photocatalysts under UV and visible light irradiation were performed according to the reported procedure [27]. The photocatalytic reaction was carried out in a 10 cm culture dish with a 14 W UV lamp and a 500 W xenon lamp covered with a UV filter fixed parallel to the reactor, respectively. MB water solution (50 ml, 10 mg/L) and 20 mg of each photocatalyst were injected into the culture dish, followed by magnetic stirring for 1 h in the dark to establish the adsorption–desorption equilibrium. Then the lamp was turned on to start the photocatalytic reaction. During the visible-light

photocatalytic reactions the temperature was maintained at ambient temperature by the flowing water in the quartz cool trap fixed around the xenon lamp. A 5 ml of the solution was taken at certain time intervals (15 min) during the measurement process and was centrifuged to remove the suspended photocatalysts completely. The absorption spectra of the MB solutions were analyzed on the UV-vis spectrophotometer.

The •OH formed on the surfaces of the irradiated photocatalysts was analyzed by the PL technique and terephthalic acid was used as the probe molecule. 2-Hydroxyterephthalic acid, a highly fluorescent compound, could be formed when terephthalic acid interacted with the produced •OH and the PL intensity was in proportion to the total •OH produced in the water solution [28,29]. The analysis procedures used were almost the same as the photocatalytic activity measurement except MB solution was replaced by the terephthalic acid water solution (1 mmol/L) with a concentration of NaOH (4 mmol/L). The PL emission spectra of 2-hydroxyterephthalic acid were recorded on the FL3-221 fluorescence spectrophotometer. The excitation and emission wavelength were 315 nm and 425 nm, respectively.

3. Results and discussion

3.1. Structures and morphologies of as-prepared photocatalysts

In order to prepare the high activity photocatalysts, CNTs, GO, and $HAuCl_4$ were used to modify the TiO_2 photocatalysts. The whole preparation strategy was summarized in Fig. 1.

The crystallographic structure of TiO_2 seeded CNTs was confirmed by the XRD shown in Fig. 2a. The diffraction peaks are a combination of the anatase TiO_2 and CNTs. The peaks ascribed to TiO_2 cannot be detected clearly which may originate from the nanocrystalline structure of TiO_2. As reported before, the TiO_2 prepared here are of anatase phase and this result can be proved by the Raman spectra (Fig. S1) [20]. The morphology of TiO_2 seeded CNTs was investigated by the FESEM and TEM. In Fig. 2b and c, nanocrystalline TiO_2 covered the whole surface of CNTs was clearly observable. A high-resolution TEM image (Fig. 1d) indicated part of a single CNT with nanocrystalized TiO_2. One set of lattice was presented with an equal lattice spacing of 0.35 nm, corresponding to the (1 0 1) atomic planes of anatase TiO_2. This result further proves the anatase phase of the TiO_2 seeds.

Fig. S2 shows the XRD pattern of GO and graphite. GO shows a characteristic peak at $2\theta = 10^{\circ}$, which is consistent with other reported results [27]. The XRD patterns (Fig. 3) of CNTs@TiO_2, CNTs@TiO_2@GP, and CNTs@TiO_2@AuGP are ascribed to the rutile phase of TiO_2. Interestingly, the disappearance of diffraction peaks of CNTs was observed, indicating the well dispersion of CNTs. Our previous study has discovered the growth of rutile TiO_2 based on the anatase TiO_2 seeds [21]. This result may be due to the

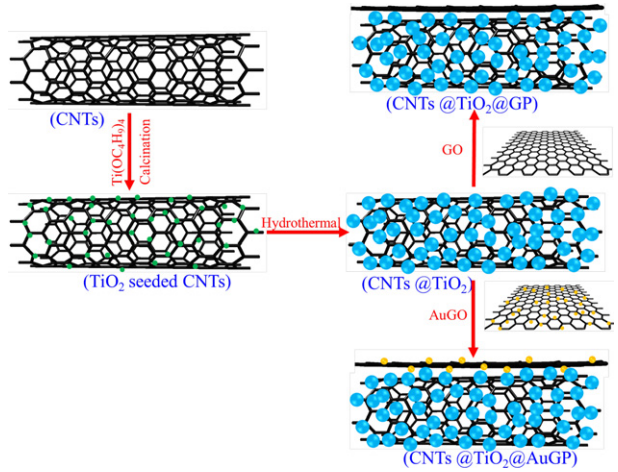

Fig. 1. A schematic illustration of the preparation of TiO_2 seeded CNTs, CNTs@TiO_2, CNTs@TiO_2@GP, and CNTs@TiO_2@AuGP.

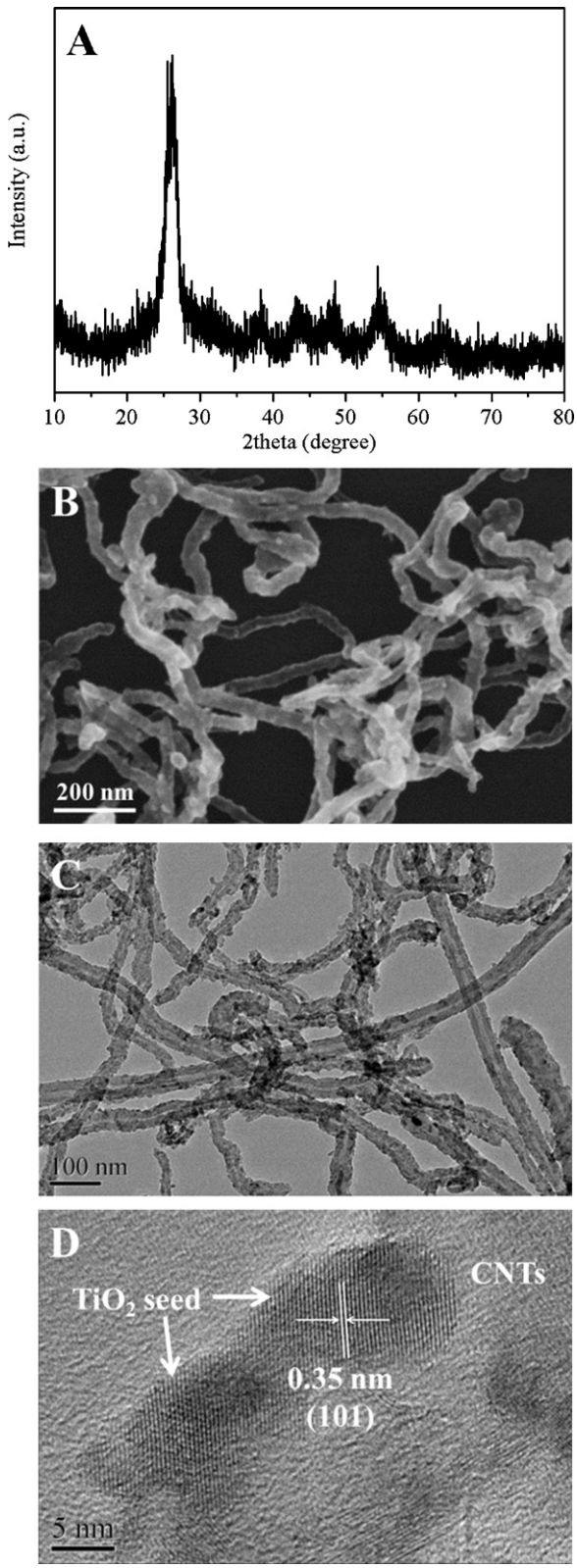

Fig. 2. (A) XRD pattern, (B) FESEM, (C) TEM, and (D) HRTEM images of TiO_2 seeded CNTs.

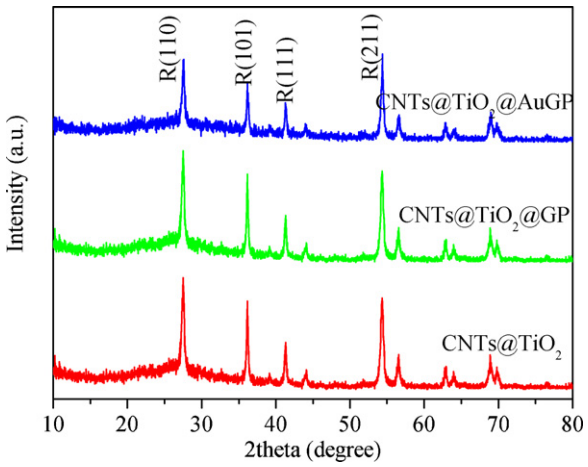

Fig. 3. XRD patterns of CNTs@TiO_2, CNTs@TiO_2@GP, and CNTs@TiO_2@AuGP.

imperfect crystal structure of the anatase TiO_2 nanoseeds and the high effect of HCl in controlling the growth of rutile TiO_2 which has also been observed by other research groups [30]. To data, systematic study on this topic is still not presented, which can be a promising research field in the future. Compared to GO, the characteristic peak disappeared in all photocatalysts, indicating GO was successfully converted to GP during the hydrothermal treatment [31]. No XRD peaks belonging to Au were detected in CNTs@TiO_2@AuGP, which may be because of that the Au particles were dispersed well on the GP and TiO_2 [13]. The peaks intensity decrement of CNTs@TiO_2@AuGP further depict that CNTs@TiO_2 are homogenously covered by the AuGP, reducing the contact between the TiO_2 particles.

FESEM and TEM analysis were used to get a direct and deeper insight on the morphology of as-prepared photocatalysts. Fig. 4a shows the typical TEM image of GO. After Au loading, the color of AuGO turned from gold to dark brown, indicating the Au particles had been deposited on the GO sheets successfully [32]. In Fig. 4b, CNTs@TiO_2 prepared with the hydrothermal method from TiO_2 seeded CNTs consisted of TiO_2 particles with the size of 100–200 nm covered on the entire surface of CNTs. This indicates that the TiO_2 particles can grow on the CNTs by previous seeds planting and the strong interaction between CNTs and TiO_2 which may be very favorable for the photocatalytic activity enhancement. Fig. 4c shows the FESEM image of CNTs@TiO_2@GP, in which GP are uniformly bonded to CNTs@TiO_2 surface. This direct interaction between CNTs, GP, and TiO_2 makes a two-channel electric conduction path on both side of TiO_2. TEM image in Fig. 4d clearly shows AuGP homogeneously anchored on CNTs@TiO_2. More importantly, some Au particles located on the GP/TiO_2 interface and some of them separately adsorbed on GP. Because of the Schottky barrier between Au and TiO_2, Au will further facilitate the transformation of the photogenerated electrons.

The FTIR spectra of TiO_2 seeded CNTs, CNTs@TiO_2, CNTs@TiO_2@GP, and CNTs@TiO_2@AuGP are given in Fig. 5. The O—H stretching vibrational modes around 3410 cm^{-1} is detected in all photocatalysts. This band can be ascribed to the surface O—H stretching vibrational of TiO_2 [33]. Compared to CNTs@TiO_2, this band moves to the higher wavenumber in CNTs@TiO_2@GP and CNTs@TiO_2@AuGP, indicating there is a strong interaction between TiO_2 and GP/AuGP. The band appearing around 1625 cm^{-1} is assigned to the C—C vibrations of CNTs and GP. The very intensive broad bands over the range of 400–800 cm^{-1} are clearly observed, which are related to the bending (633 cm^{-1}) and stretching (524 cm^{-1}) vibrational modes of Ti—O—Ti bonds [34]. The peak at ~1015 cm^{-1} assigned to the C—O stretching mode is appeared in

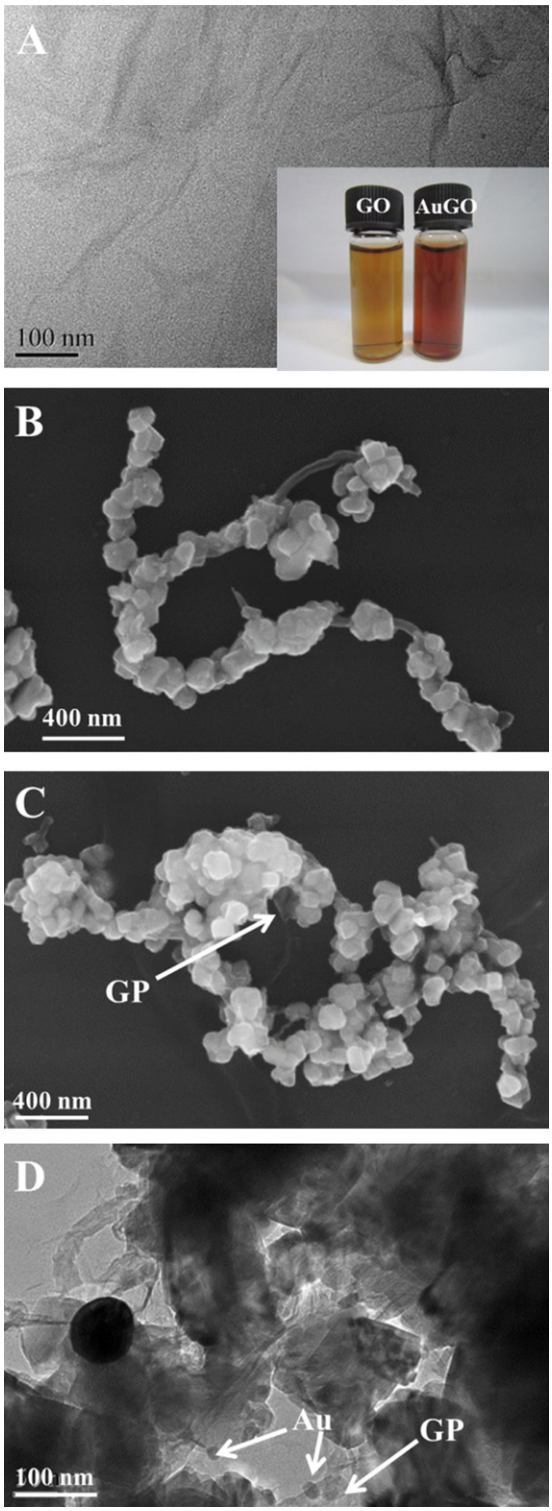

Fig. 4. (A) TEM image of GO and colors of GO and AuGO (inset), FESEM images of (B) CNTs@TiO_2 and (C) CNTs@TiO_2@GP, and (D) TEM image of CNTs@TiO_2@AuGP.

TiO_2 seeded CNTs and CNTs@TiO_2. As discussed in the FESEM analysis, TiO_2 is covered on the entire surface of CNTs, thus the Ti—O—C chemical bond may be formed [33]. The same peak appearing in CNTs@TiO_2@GP and CNTs@TiO_2@AuGP may also originate from the same above mentioned conditions. However, some of them may also originate from the GP and AuGP as the hydrothermal treatment cannot reduce the GO and AuGO completely. To make a deep illustration on this point, C 1s XPS spectra of CNTs@TiO_2@GP

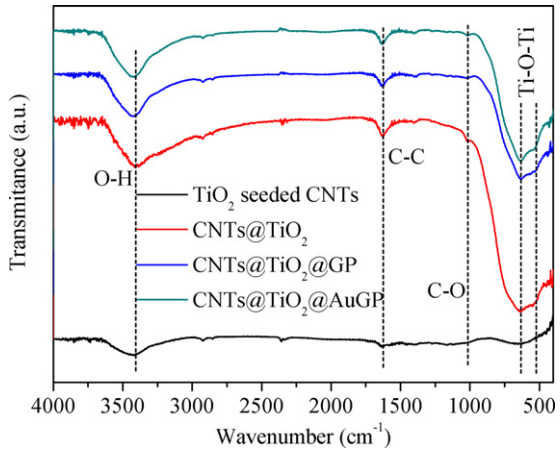

Fig. 5. FTIR spectra of TiO_2 seeded CNTs, CNTs@TiO_2, CNTs@TiO_2@GP, and CNTs@TiO_2@AuGP.

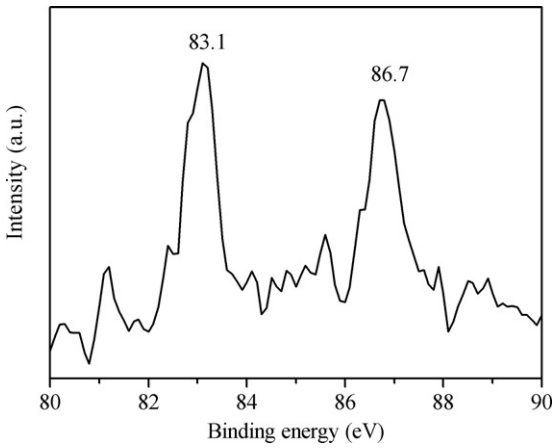

Fig. 7. Au 4f XPS spectra of CNTs@TiO_2@AuGP.

and CNTs@TiO_2@AuGP are given in Fig. 6a and b. The peak centered at 284.6 eV is attributed to the sp^2 and sp^3 carbon species, while the peaks centered at 285 eV, 286.1 eV, and 288.5 eV are attributed to the C—OH, C—O, and O=C—O species [32,35]. The appearance of C—OH and O=C—O chemical bonds may indicate that GO and AuGO were not completely reduced. The XRD analysis did not detect this result may be because of the highly homogeneous dispersion of GP and AuGP, which can be proved by the FESEM and TEM analysis. After the formation of CNTs@TiO_2@AuGP composite, the peak intensity of C—OH decreased significantly, which indicates that GO in CNTs@TiO_2@AuGP was deeper reduced to GP than that in CNTs@TiO_2@GP. This further reduction is very favorable for the electrons transfer, resulting in higher conductivity [36]. On the other hand, the residue of O=C—O and C—OH bonds could serve as bridges to enhance the interaction between TiO_2 and GP [17].

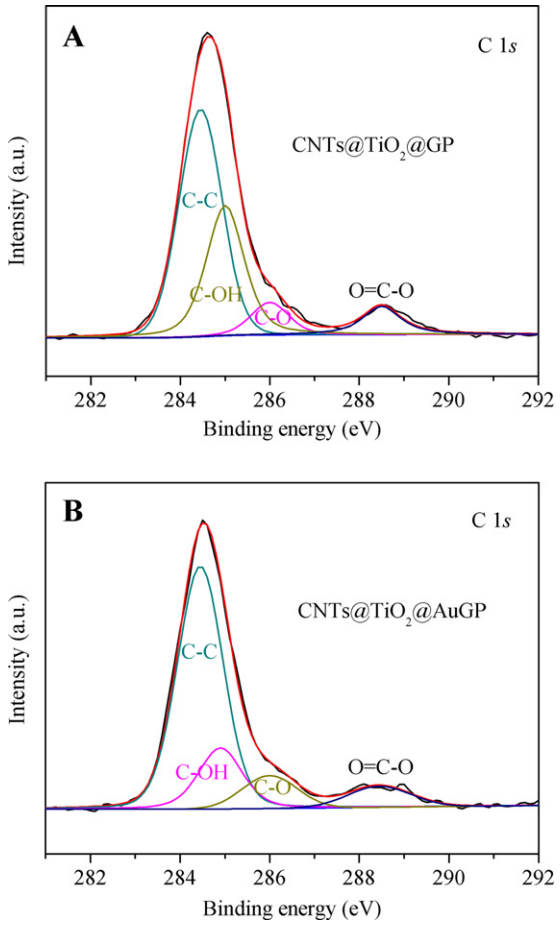

Fig. 6. C 1s XPS spectra of (A) CNTs@TiO_2@GP and (B) CNTs@TiO_2@AuGP.

The chemical environment of Au particles loaded on CNTs@TiO_2@AuGP was also investigated. As shown in Fig. 7, the core line is centered at 83.1 eV (Au $4f_{7/2}$) and the spin orbit separations are 3.6 eV, indicating the Au loaded are in the form of Au^0 [13,37,38]. As the GP in CNTs@TiO_2@AuGP is deeper reduced, the difference between the reduction potential of $AuCl_4^{-1}$ and the oxidation potential of GO may be the driving force of Au deposition [32]. However, the binding energy of Au $4f_{7/2}$ in CNTs@TiO_2@AuGP is lower than that of pure Au foil (84 eV). Li et al. considered this negative shift is due to the strong metal-support interaction [39]. As discussed in the TEM analysis, the Au particles are located on the surface of TiO_2 and GP, the electrons transfer from TiO_2 may lead to the lower core-level binding energy of Au in CNTs@TiO_2@AuGP [13,40]. This interaction among Au, GP, and CNTs@TiO_2 would be beneficial for the photocatalytic activity enhancement over CNTs@TiO_2@AuGP.

Raman spectroscopy was also used to provide information on the structure of the samples. Fig. 8a shows the TiO_2 Raman spectra of TiO_2 seeded CNTs, CNTs@TiO_2, CNTs@TiO_2@GP, and CNTs@TiO_2@AuGP. TiO_2 seeded CNTs gives a very weak Raman spectrum (Fig. S1), suggesting the low crystalline property of TiO_2 which is consistent with the XRD analysis. The Raman active 148 cm^{-1} (B_{1g}), 245 cm^{-1} (complex band), 428 cm^{-1} (E_g), 608 cm^{-1} (A_{1g}), and 832 cm^{-1} (B_{2g}) modes for the composites match with the structure of rutile TiO_2 [41]. In addition, the peak corresponding to the E_g mode for CNTs@TiO_2@AuGP is red-shifted from 428 cm^{-1} to 435 cm^{-1}. The peak position of the Raman spectrum is mainly affected by the crystal structures [42,43]. In this investigation, the same laser source was used for recording the Raman spectra. As a result, the Raman shift of CNTs@TiO_2@AuGP is resulted from the different crystal structure [31]. As reported before in the condition of CNTs modified TiO_2, this result clearly indicates that the deposition of Au particle displays a strong chemical interaction between AuGP and CNTs@TiO_2 [44]. This structure is very essential for efficient photogenerated electron transfer.

Fig. 8b shows the Raman spectra of carbon species presented in the photocatalysts. It is well known that the D and G bands are the feature of sp^3 defects in carbon and in plane vibrations of sp^2 bonded carbons, respectively [45]. Three features can be obtained to illustrate the structure change in the photocatalysts during the preparation process. First, the shift of the D and G band in CNTs@TiO_2 compared to that in TiO_2 seeded CNTs. This

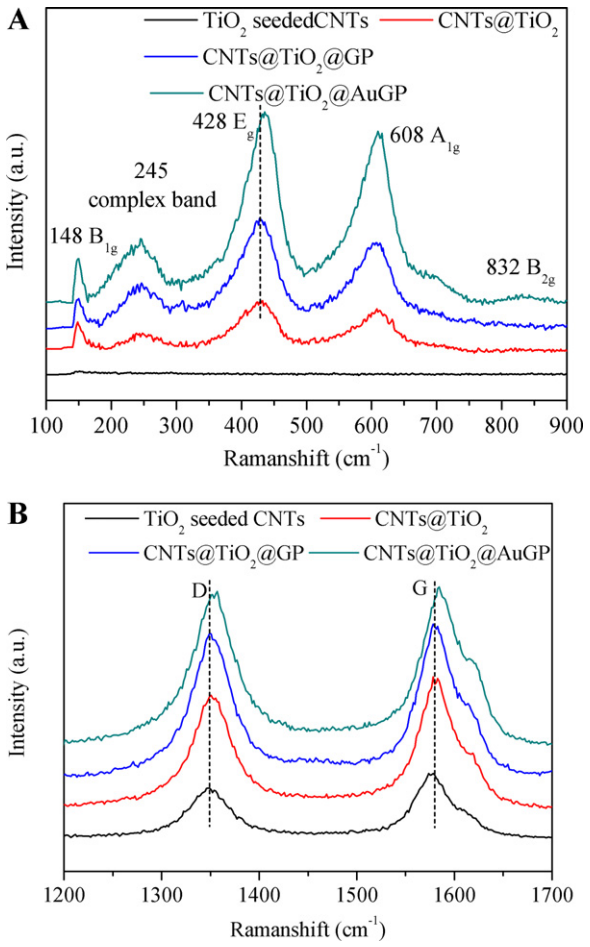

Fig. 8. Raman spectra of (A) TiO_2 and (B) carbon species in TiO_2 seeded CNTs, CNTs@TiO_2, CNTs@TiO_2@GP, and CNTs@TiO_2@AuGP.

indicates that there is a new and strong interaction between the CNTs and TiO_2, which may due to the change of the TiO_2 structure and the bonds (Ti—O—C) between TiO_2 and CNTs. Second, the intensity ratio of the D band to the G band changes in CNTs@TiO_2@GP and CNTs@TiO_2@AuGP. The calculated I_D/I_G in CNTs@TiO_2@GP and CNTs@TiO_2@AuGP are 0.9587 and 0.9799, respectively. The increase in the I_D/I_G ratio suggests the decrease in the number of GP layers, which means the location of Au particles facilitate the separation of the GP layers [31,46]. The decrease of the GP layers is an essential factor in enhancing the conductivity of GP, thus the photocatalytic activity of the photocatalyst can be improved. Third, the shift of the D and G bands in CNTs@TiO_2@AuGP compared to that in CNTs@TiO_2@GP. As discussed in the C 1s XPS spectra, the GP in CNTs@TiO_2@AuGP is deeper reduced than that in CNTs@TiO_2@GP. The shift of the D and G bands may also indicate the higher conversion of GO to GP [46]. Therefore, all these changes in Raman spectra provide clear evidence for the strong interaction between CNTs and TiO_2, the presence of GP, and the vital effect of Au loading.

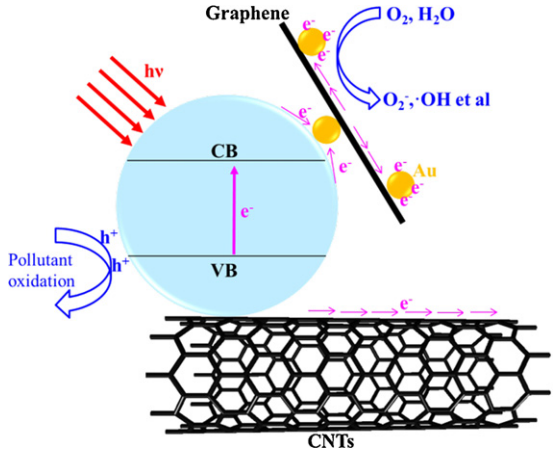

Fig. 9. The proposed photocatalytic mechanisms for CNTs@TiO_2@AuGP.

3.2. Photocatalytic activity measurements

Organic dyes which often regarded as environment contaminants are widely used in a variety of fields. In this work, the photocatalytic activity of the photocatalysts was measured by the degradation of MB under the UV and visible light irradiation, respectively. The photocatalysis mechanisms are shown in Fig. 9. After the TiO_2 particle is irradiated by the light with energy higher than its band gap, electrons will be excited from the valence band (VB) to the conduction band (CB). Then the electrons will transfer to the surface of the photocatalysts and react with O_2, H_2O et al. to form radical species. Both the radical species and the located holes will react with the absorbed organic pollutants. It is known that the fast recombination of the electrons and holes limits the photocatalysis reaction significantly [5]. In the present study, the present of CNTs, GP, and Au efficiently resolve this point. On one hand, the strong interaction between the high conductive CNTs and TiO_2 will transfer the electrons from the inner side of TiO_2 to prevent the

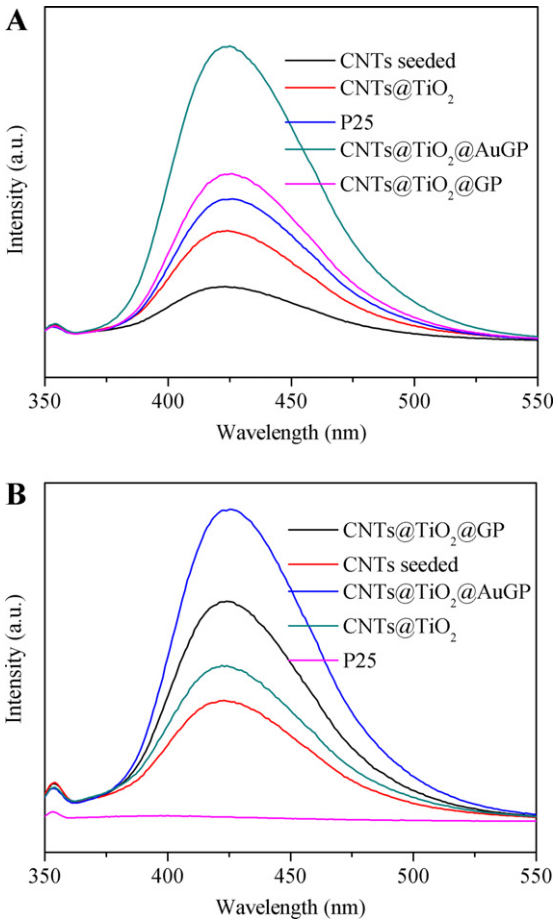

Fig. 10. PL spectra of 2-hydroxyterephthalic acid in the solutions based on P25, TiO_2 seeded CNTs, CNTs@TiO_2, CNTs@TiO_2@GP, and CNTs@TiO_2@AuGP under (A) UV and (B) visible light irradiation for 90 min.

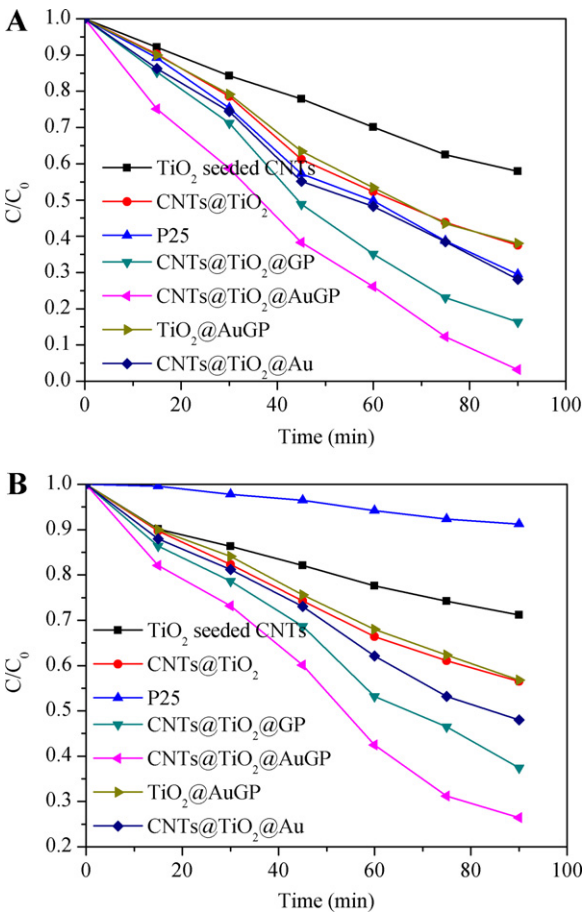

Fig. 11. Photocatalytic degradation of MB under the (A) UV and (B) visible light ($\lambda > 400$ nm) irradiation over P25, TiO_2 seeded CNTs, CNTs@TiO_2, TiO_2@AuGP, CNTs@TiO_2@Au, CNTs@TiO_2@GP, and CNTs@TiO_2@AuGP.

fast recombination of electrons and holes. On the other hand, the GP covered on the surface of TiO_2 are also very essential for the electrons transformation. In CNTs@TiO_2@AuGP, the deposition of Au particle forms a Schottky barrier at the Au/TiO_2 interface, which will drive the electrons transfer from TiO_2 to Au [47,48]. Because of the Au also located on the GP, the collected electrons on the Au particles will migrate onto the GP and the Au particles on the other side of the GP. Thus, a lot of radical species are formed and most of the holes can also diffuse to the TiO_2 surface to oxide the pollutants.

Fig. 10a and b shows a comparison of the PL spectra of terephthalic acid solution with different photocatalysts under UV and visible light irradiation for 90 min, respectively. It is known that the PL intensity is proportional to the amount of generated •OH [49,50]. Obviously, CNTs@TiO_2@AuGP gives the largest amount of •OH among all the photocatalysts. This result implies that the electrons and holes are efficiently separated by the CNTs, GP, and Au particles. The lower PL intensity in the solution containing CNTs@TiO_2@GP further suggests the essential effect of Au. The lower PL intensity of TiO_2 seeded CNTs than that of CNTs@TiO_2 may result from that there are less TiO_2 particles and more defects in the nanocrystalline TiO_2 in TiO_2 seeded CNTs. Further observation show that P25 shows no PL signal under visible light irradiation, which is in consistent with its band structure. The •OH analysis also confirms that the electrons can form active species during the photocatalytic reactions.

The photocatalytic activity efficiency measurements of the photocatalysts are based on the theories reported before [36]. As a result, the degradation efficiency spectra of MB under the UV and visible light irradiation, respectively, are described in Fig. 11a and b. To confirm the superiority of the "two-channel electron conduction path", TiO_2@AuGP and CNTs@ TiO_2@Au were also tested as the reference photocatalysts. When the reactions were conducted under the UV light, CNTs@TiO_2, CNTs@TiO_2@Au, and TiO_2@AuGP show similar photoactivity, and CNTs@TiO_2@AuGP and CNTs@TiO_2@GP all give higher degradation ability than other photocatalysts, including P25. The highest efficiency of CNTs@TiO_2@AuGP confirms the superiority of its structure than the rest photocatalysts. In contrast, P25 gives the lowest efficiency in the degradation of MB under the visible light irradiation, which may be due to its large band gap. For TiO_2 seeded CNTs, there are only a little nanocrystalline TiO_2 located on the surface of CNTs and the electrons and holes will recombine easily in the bulk of TiO_2 for there are too much defects located. Thus, the photocatalytic activity of TiO_2 seeded CNTs is lower than that of CNTs@TiO2. The photocatalysis efficiency order of CNTs@TiO_2, CNTs@TiO_2@GP, and CNTs@TiO_2@AuGP is also consistent with the •OH analysis and the light absorption spectra (Fig. S3). The improved photocatalysis efficiency of the CNTs@TiO_2@AuGP compared to that of CNTs@TiO_2@GP and CNTs@TiO_2 can be further detected by the PL spectra analysis. The PL spectra are very efficient in studying the surface electron and hole's recombination process of TiO_2 [51,52]. As shown in Fig. S4, the addition of GP and AuGP will lead to the PL quenching of CNTs@TiO_2 gradually, indicating much more efficient inhibition of electrons and holes' recombination which is very favorable for photocatalytic activity enhancement. This seems well consistent with the •OH and photocatalytic activity analysis.

4. Conclusions

In summary, we have for the first time reported a systematic study on enhancing the photocatalytic activity of TiO_2 via photocatalyst structure design. This approach allows us to make efficient use of the solar light and the electron conductivity of Au, CNTs, and GP, thereby inhibit the recombination of photogenerated electron–hole pair over the modified photocatalysts upon both UV and visible light irradiation. This induces the significant photocatalytic activity improvement of CNTs@TiO_2@GP and CNTs@TiO_2@AuGP toward decomposing organic pollutants under natural conditions. This structure design strategy can be used to prepare other CNTs and GP modified photocatalysts for various applications. Our present work emphasizes the importance of fabrication photocatalysts with two-channel electron conduction path structures combing with the Schottky barrier toward contaminants decomposition. Our research would significantly advance the design and synthesis of noble metals, CNTs, and GP modified heterogeneous photocatalysts to make efficient use of solar energy to aimed applications.

Acknowledgments

This work was supported by the Innovation Foundation for Graduate Students of Jiangsu Province China (CXLX11_0346) and a project funded by the Priority Academic Program Development of Jiangsu Higher Education Institutions (PAPD).

Appendix A. Supplementary data

Supplementary data associated with this article can be found, in the online version, at http://dx.doi.org/10.1016/j.apcatb.2012.10.014.

References

[1] A. Fujishima, K. Honda, Nature 238 (1972) 37–38.
[2] A. Fujishima, X. Zhang, D.A. Tryk, Surface Science Reports 63 (2008) 515–582.

[3] S. Liu, C. Liu, W. Wang, B. Cheng, J. Yu, Nanoscale 4 (2012) 3193–3200.
[4] R. Asahi, T. Morikawa, T. Ohwaki, K. Aoki, Y. Taga, Science 293 (2001) 269–271.
[5] D.Y.C. Leung, X. Fu, C. Wang, M. Ni, M.K.H. Leung, X. Wang, X. Fu, ChemSusChem 3 (2010) 681–694.
[6] C.-C. Tsai, H. Teng, Applied Surface Science 254 (2008) 4912–4918.
[7] Y. Zhang, S.G. Ebbinghaus, A. Weidenkaff, T. Kurz, H.-A. Krug von Nidda, P.J. Klar, M. Güngerich, A. Reller, Chemistry of Materials 15 (2003) 4028–4033.
[8] A.M. Czoska, S. Livraghi, M. Chiesa, E. Giamello, S. Agnoli, G. Granozzi, E. Finazzi, C.D. Valentin, G. Pacchioni, Journal of Physical Chemistry C 112 (2008) 8951–8956.
[9] H. Wang, Z. Wu, Y. Liu, Journal of Physical Chemistry C 113 (2009) 13317–13324.
[10] H. Zhu, B. Yang, J. Xu, Z. Fu, M. Wen, T. Guo, S. Fu, J. Zuo, S. Zhang, Applied Catalysis B: Environmental 90 (2009) 463–469.
[11] J. Zhang, P. Du, J. Schneider, P. Jarosz, R. Eisenberg, Journal of the American Chemical Society 129 (2007) 7726–7727.
[12] E. Kowalska, R. Abe, B. Ohtani, Chemical Communications (2009) 241–243.
[13] S. Zhu, S. Liang, Q. Gu, L. Xie, J. Wang, Z. Ding, P. Liu, Applied Catalysis B: Environmental 119–120 (2012) 146–155.
[14] J.S. Jang, S.H. Choi, H.G. Kim, J.S. Lee, Journal of Physical Chemistry C 112 (2008) 17200–17205.
[15] S. Zhang, H. Niu, Y. Lan, C. Cheng, J. Xu, X. Wang, Journal of Physical Chemistry C 115 (2011) 22025–22034.
[16] B. Liu, H.C. Zeng, Chemistry of Materials 20 (2008) 2711–2718.
[17] J. Zhang, Z. Xiong, X.S. Zhao, Journal of Materials Chemistry 21 (2011) 3634–3640.
[18] B.K. Vijayan, N.M. Dimitrijevic, D. Finkelstein-Shapiro, J. Wu, K.A. Gray, ACS Catalysis 2 (2011) 223–229.
[19] Y. Lin, D.W. Baggett, J.-W. Kim, E.J. Siochi, J.W. Connell, ACS Applied Materials & Interfaces 3 (2011) 1652–1664.
[20] Y.-J. Xu, Y. Zhuang, X. Fu, Journal of Physical Chemistry C 114 (2010) 2669–2676.
[21] W. Wang, C. Lu, Y. Ni, M. Su, Z. Xu, Materials Letters 79 (2012) 11–13.
[22] A.K. Geim, Science 324 (2009) 1530–1534.
[23] Y. Zhang, Z.-R. Tang, X. Fu, Y.-J. Xu, ACS Nano 5 (2011) 7426–7435.
[24] T. Xu, L. Zhang, H. Cheng, Y. Zhu, Applied Catalysis B: Environmental 101 (2011) 382–387.
[25] W.S. Hummers, R.E. Offeman, Journal of the American Chemical Society 80 (1958) 1339.
[26] L. Shen, X. Zhang, H. Li, C. Yuan, G. Cao, Journal of Physical Chemistry Letters 2 (2011) 3096–3101.
[27] Y. Zhang, Z.-R. Tang, X. Fu, Y.-J. Xu, ACS Nano 4 (2010) 7303–7314.
[28] J. Yu, B. Wang, Applied Catalysis B: Environmental 94 (2010) 295–302.
[29] J. Yu, W. Wang, B. Cheng, B.-L. Su, Journal of Physical Chemistry C 113 (2009) 6743–6750.
[30] R. Zou, Z. Zhang, L. Yu, Q. Tian, Z. Chen, J. Hu, Chemistry: A European Journal 17 (2011) 13912–13917.
[31] S.D. Perera, R.G. Mariano, K. Vu, N. Nour, O. Seitz, Y. Chabal, K.J. Balkus, ACS Catalysis 2 (2012) 949–956.
[32] N. Zhang, H. Qiu, Y. Liu, W. Wang, Y. Li, X. Wang, J. Gao, Journal of Materials Chemistry 21 (2011) 11080–11083.
[33] Y. Wen, H. Ding, Y. Shan, Nanoscale 3 (2011) 4411–4417.
[34] N.T. McDevitt, W.L. Baun, Spectrochimica Acta 20 (1964) 799–808.
[35] S. Yumitori, Journal of Materials Science 35 (2000) 139–146.
[36] L. Sun, Z. Zhao, Y. Zhou, L. Liu, Nanoscale 4 (2012) 613–620.
[37] B. Tian, J. Zhang, T. Tong, F. Chen, Applied Catalysis B: Environmental 79 (2008) 394–401.
[38] J. Huang, W.-L. Dai, H. Li, K. Fan, Journal of Catalysis 252 (2007) 69–76.
[39] H. Li, Z. Bian, J. Zhu, Y. Huo, H. Li, Y. Lu, Journal of the American Chemical Society 129 (2007) 4538–4539.
[40] N. Kruse, S. Chenakin, Applied Catalysis A-General 391 (2011) 367–376.
[41] G.A. Tompsett, G.A. Bowmaker, R.P. Cooney, J.B. Metson, K.A. Rodgers, J.M. Seakins, Journal of Raman Spectroscopy 26 (1995) 57–62.
[42] S. Balaji, Y. Djaoued, J. Robichaud, Journal of Raman Spectroscopy 37 (2006) 1416–1422.
[43] S. Sahoo, A.K. Arora, V. Sridharan, Journal of Physical Chemistry C 113 (2009) 16927–16933.
[44] S. Dora, V.-S. Enrique, H.-L. Susana, G.-C. Antonio, A.-F. Manuel, C.-L. Marco Antonio, Science and Technology of Advanced Materials 9 (2008) 025003.
[45] R. Rao, R. Podila, R. Tsuchikawa, J. Katoch, D. Tishler, A.M. Rao, M. Ishigami, ACS Nano 5 (2011) 1594–1599.
[46] I.-S. Yoon, C.-D. Kim, B.-K. Min, Y.-K. Kim, B.-S. Kim, W.-S. Jung, Bulletin of the Korean Chemical Society 30 (2009) 3045–3048.
[47] A.L. Linsebigler, G. Lu, J.T. Yates, Chemical Reviews 95 (1995) 735–758.
[48] J. Bisquert, A. Zaban, P. Salvador, Journal of Physical Chemistry B 106 (2002) 8774–8782.
[49] J. Yu, L. Shi, Journal of Molecular Catalysis A: Chemical 326 (2010) 8–14.
[50] Q. Xiang, J. Yu, M. Jaroniec, Physical Chemistry Chemical Physics 13 (2011) 4853–4861.
[51] Y.T. Liang, B.K. Vijayan, K.A. Gray, M.C. Hersam, Nano Letters 11 (2011) 2865–2870.
[52] Y. Yao, G. Li, S. Ciston, R.M. Lueptow, K.A. Gray, Environmental Science and Technology 42 (2008) 4952–4957.